Comparative Studies on the Primary-Side Frequency and Phase Shift Control for Series-Series Compensated Inductive Power Transfer

Lit Hong Chan[1], Yun Yang[2], Ka-wai Eric Cheng[3]
1. Department of Electrical Engineering, The Hong Kong Polytechnic University, Hong Kong, kenchan1012@gmail.com.
2. Department of Electrical Engineering, The Hong Kong Polytechnic University, Hong Kong, yun1989.yang@polyu.edu.hk.
3. Department of Electrical Engineering, The Hong Kong Polytechnic University, Hong Kong, eric-cheng.cheng@polyu.edu.hk.

Abstract–Since the Society of Automobile Engineers (SAE) launched the guideline J2954 for wireless battery charging of electric vehicles (EVs), research activities on inductive power transfer (IPT) or wireless power transfer (WPT) in EVs are intensified over the last few years. The guideline J2954 calls for an operating frequency around 85 kHz and power at four levels. In this paper, both frequency and phase shift control, are designed by controlling the front-end inverters to achieve constant current (CC) and constant voltage (CV) control of Li-ion battery loads in a power-scaled-down (i.e., 200 W) IPT system. Simulation results using PSIM9.0 have verified the effectiveness of both control strategies.APEJ vol.14

Keywords-Inductive power transfer (IPT), efficiency, frequency control, phase shift control.

I. Introduction

Due to the convenience and safety, inductive power transfer (IPT) technology is gaining increasing attentions in recent years and has been widely used for portable electronics, electric vehicles (EVs), and implantable biomedical devices [1]-[3]. Thereinto, the Li-ion batteries are most widely adopted energy storages for IPT systems. Generally, the charging strategy for the Li-ion batteries comprise a constant current (CC) charging first and then a constant voltage (CV) second to prevent the degradation of the lifespans. Specifically, the Li-ion batteries are recommended to be charged in the CC mode when the state-of-charge (SoC) or the output voltage is below a threshold (e.g., 90% or 4.2 V). However, when the SoC or the output voltage is above the threshold, the Li-ion batteries are required to be charged in the CV mode. By far, various efforts have been made to achieve the CC and CV charging [4]-[15]. In [4]-[6], DC-DC converters are used at the receiver sides to implement the CC and CV charging. However, extra power losses are inevitable, which result in reduced efficiencies and large volumes. In [7]-[15], front-end control methods based on the communication-free observers at the primary sides are proposed. The front-end controllers can accurately control the output currents and the output voltages at the nominal conditions, while the robustness of the proposed controllers is quite low. To address these issues, two feedback control, i.e., frequency and phase shift control, are the most reliable and efficient control strategies for the CC and CV charging of battery loads in IPT systems [4], [7].

Frequency control is achieved by regulating the switching frequency of the primary-side inverter based on the feedbacks of the charging current and the charging voltage of the battery load. By changing the switching frequency, the impedances of both the transmitting and the receiving resonators can be altered. As a result, the charging current and the charging voltage can be regulated. Phase shift control is implemented by delaying an angle between the two bridge arms. By changing the phase shift angle, the fundamental component of the input voltage of the transmitter can be altered. Consequently, the charging current and the charging voltage can be regulated. The prominent advantage of the phase shift control is that the IPT system can always be operated at the resonant frequency.

This paper aims to implement both frequency and phase shift control for series-series (SS)-compensated IPT systems. Based on comprehensive analysis of the systems with different mutual inductances and load conditions, simulations are carried out in PSIM9.0 to exhibit the applications of both control strategies for an 85kHz IPT system with the power rating about 200 W. Nevertheless, the control designs are also validated for general IPT systems.

II. Analysis of the Frequency and Phase Shift Control

The circuit diagram of an SS-compensated IPT system with feedback control is depicted in Fig. 1. The input DC voltage is V_{dc}. A full-bridge inverter is adopted to drive the transmitter resonator. Both C_p and C_s are designed in resonances with L_p and L_s as

$$\omega^2 = \frac{1}{L_p C_p} = \frac{1}{L_s C_s} \quad (1)$$

where ω is the switching angular frequency. At the receiver side, a diode-bridge rectifier and a filter capacitor C_f are adopted to feed DC current and voltage for the battery load. Without using a DC regulator at the user-end, the power density, reliability and cost of the receiver circuit can be improved. However, to regulate the charging current in the CC mode and the charging voltage in the CV mode, wired or wireless communications are required between the transmitter and receiver. As shown in Fig. 1, the measured output current (i.e., I_o) and output voltage (i.e., V_o) are fed back to the primary-side controller to regulate the front-end inverter.

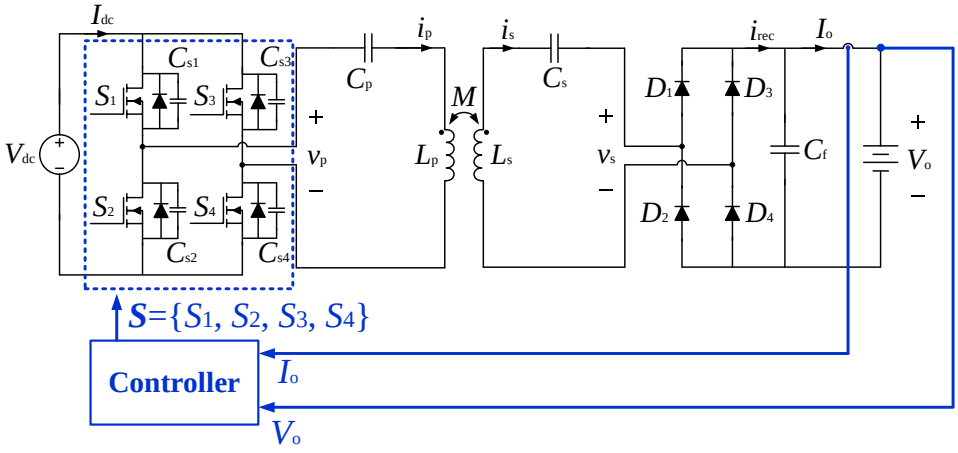

Fig. 1: An SS-compensated IPT system with direct feedback control.

Generally, two types of controllers (i.e., frequency and phase shift control) are most widely adopted for the inverters of IPT systems. Based on the circuit diagram in Fig. 1, the equivalent circuit at the fundamental frequency of the system can be plotted, as shown in Fig. 2. Due to the filtering by the resonators, only the fundamental components v_{p1}, i_{p1}, v_{s1} and i_{s1} are considered in the equivalent circuit. Based on the Kirchhoff's circuit laws,

$$v_{p1} = Z_p i_{p1} - j\omega M i_{s1} \quad (2.1)$$

$$j\omega M i_{p1} = (Z_s + R_L') i_{s1} \quad (2.2)$$

where $Z_p = j\omega L_p + \frac{1}{j\omega C_p} + R_p$ and $Z_s = j\omega L_s + \frac{1}{j\omega C_s} + R_s$. R_p and R_s are the equivalent-series-resistances (ESRs). M is the mutual inductance. R_L' is the equivalent resistance of the rectifier, filter (i.e., C_f), and the battery. During the charging process, the battery load can be modelled as a resistive load R_L. Based on the Fourier analysis,

$$R_L' = \frac{8}{\pi^2} R_L \quad (3)$$

By substituting (3) into (2.2) and eliminating i_{p1} in both (2.1) and (2.2), the charging current and charging voltage of the equivalent circuit, i.e., i_{s1} and v_{s1}, can be derived as

$$i_{s1} = \frac{\pi^2 \omega M}{\pi^2(Z_p Z_s + \omega^2 M^2) + 8 Z_p R_L} v_{p1} j \quad (4.1)$$

$$v_{s1} = \frac{8\omega M R_L}{\pi^2(Z_p Z_s + \omega^2 M^2) + 8 Z_p R_L} v_{p1} j \quad (4.2)$$

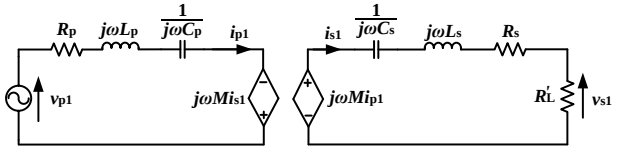

Fig. 2: Equivalent circuit at fundamental frequency.

A. *Frequency Control*

For the frequency control, the switching signals S_1 and S_2, S_3 and S_4 are complimentary and the switching signals S_1 and S_4, S_2 and S_3 are in phase. The timing diagrams of the four gate signals are depicted in Fig. 3.

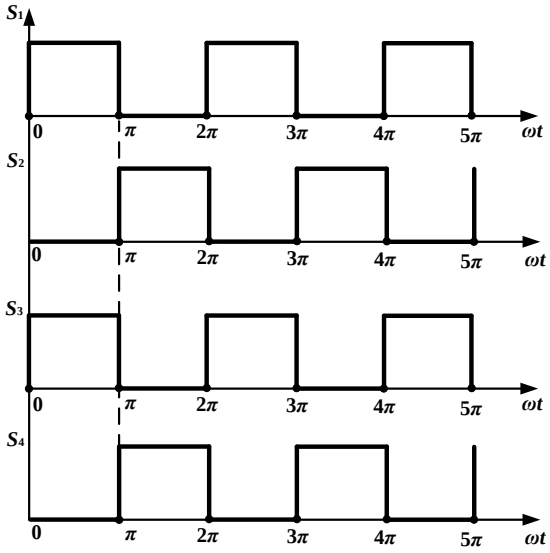

Fig. 3: Timing diagrams of the gate signals of the frequency control.

Therefore, based on the Fourier analysis,

$$I_{p1} = \frac{\pi}{2} I_{dc} \quad (5.1)$$

$$V_{p1} = \frac{4}{\pi} V_{dc} \quad (5.2)$$

where V_{p1} and I_{p1} are the peak values of v_{p1} and i_{p1}, respectively. Similarly, the charging current and charging voltage can be derived as

$$I_{s1} = \frac{\pi}{2} I_o \quad (6.1)$$

$$V_{s1} = \frac{4}{\pi} V_o \quad (6.2)$$

By substituting (5.2), (6.1) and (6.2) into (4.1) and (4.2), respectively,

$$I_o = \left| \frac{8\omega M V_{dc}}{\pi^2(Z_p Z_s + \omega^2 M^2) + 8 Z_p R_L} \right| \quad (7.1)$$

$$V_o = \left| \frac{8\omega M R_L V_{dc}}{\pi^2(Z_p Z_s + \omega^2 M^2) + 8 Z_p R_L} \right| \quad (7.2)$$

Apparently, the output charging current and the output charging voltage can be regulated by the switching angular frequency ω.

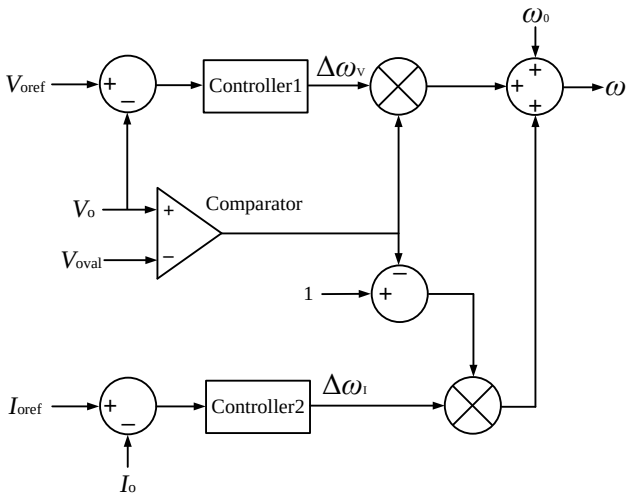

Fig. 4: Schematic diagram of the frequency control.

The schematic diagram of the frequency control is depicted in Fig. 4. Here, V_{oref} and I_{oref} are the output voltage and output current references. The controller1 and controller2 are used to track the voltage and current references, respectively. The outputs of the controller1 and controller2 are $\Delta\omega_V$ and $\Delta\omega_I$, respectively. The output of the frequency control is the addition of $\Delta\omega_V$, $\Delta\omega_I$ and ω_0, where ω_0 is the nominal angular frequency. When V_o is below the threshold (i.e. V_{oval}), the controller2 operates at the CC charging mode, such that the output of the comparator is null. Thus, the output of the frequency control only comprises $\Delta\omega_I$ and ω_0. Similarly, when the battery voltage (i.e., V_o) is above the threshold (i.e. V_{oval}), the controller1 operates at the CV charging mode, such that the output of the comparator is one. Therefore, the output of the frequency control only comprises $\Delta\omega_V$ and ω_0.

B. Phase Shift Control

For the phase shift control, the output current and the output voltage are controlled by changing the phase shift angle between the switching signals S_1 and S_4, S_2 and S_3, while S_1 and S_2, S_3 and S_4 are complimentary. The timing diagrams of the four gate signals are depicted in Fig. 5.

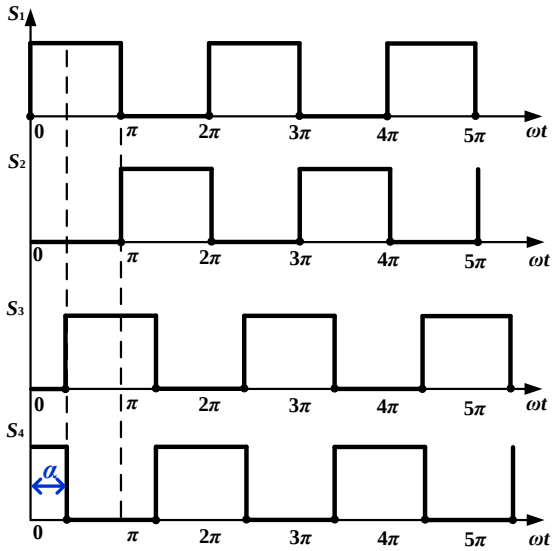

Fig. 5: Timing diagrams of the gate signals of the phase shift control.

Based on the Fourier analysis,

$$V_{p1} = \frac{4}{\pi} V_{dc} \cos\left(\frac{\alpha}{2}\right) \tag{8}$$

By substituting (6.1), (6.2) and (8) into (4.1) and (4.2), respectively,

$$I_o = \left| \frac{8\omega M V_{dc} \cos\left(\frac{\alpha}{2}\right)}{\pi^2 (Z_p Z_s + \omega^2 M^2) + 8 Z_p R_L} \right| \tag{9.1}$$

$$V_o = \left| \frac{8\omega M R_L V_{dc} \cos\left(\frac{\alpha}{2}\right)}{\pi^2 (Z_p Z_s + \omega^2 M^2) + 8 Z_p R_L} \right| \tag{9.2}$$

Apparently, the output current and the output voltage can be regulated by the phase shift angle α.

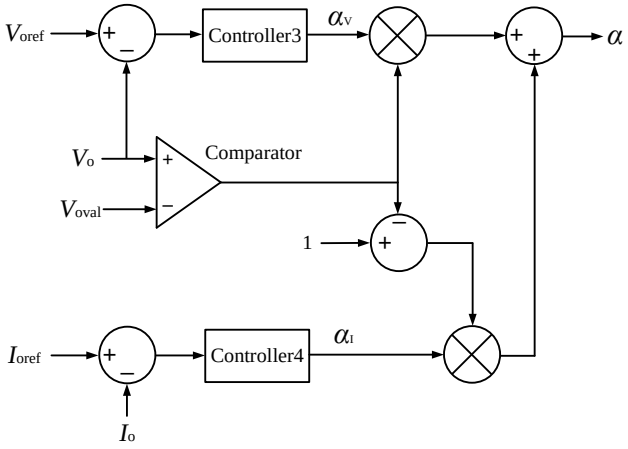

Fig. 6: Schematic diagram of the phase shift control.

The schematic diagram of the phase shift control is depicted in Fig. 6. The outputs of the controller3 and controller4 are α_V and α_I, respectively. The output of the phase control is the addition of α_V and α_I. When the battery voltage (i.e., V_o) is below the threshold (i.e. V_{oval}), the controller4 operates at the CC charging mode, such that the output of the comparator is null. Thus, the output of the phase shift control is α_I. Similarly, when the battery voltage (i.e., V_o) is above the threshold (i.e. V_{oval}), the controller3 operates at the CV charging mode, such that the output of the comparator is one. Thus, the output only comprises α_V and α_I.

III. Simulation Results

The parameters of the IPT system in simulation (PSIM9.0) are listed in Table I. The current control and voltage control of both control strategies (i.e., Controller1, Controller2, Controller3, and Controller4) in Figs. 4 and 6 are implemented by proportional-integral (PI) control. The control parameters are given in Table II. The nominal charging current and charging voltage are 12 A and 60 V, respectively.

Table 1: Specifications of the IPT system in simulation

Parameter	Symbol	Value
Nominal frequency	f_0	85 kHz
DC voltage source	V_{dc}	132 V
Parasitic capacitances of the inverter switches	C_{s1}, C_{s2}, C_{s3}, C_{s4}	315 pF
Transmitter coil inductance	L_p	91.78 μH
Receiver coil inductance	L_s	92.05 μH
Transmitter compensated capacitance	C_p	49 nF
Receiver compensated capacitance	C_s	49 nF

ESR of the transmitter	R_p	0.7 Ω
ESR of the Receiver	R_s	0.8 Ω
Forward voltage of the diode in the rectifier	V_D	0.5 V
Filter capacitance	C_f	100 μF
Nominal battery load equivalent resistance	R_L	5 Ω
Nominal mutual inductance	M	19.34 μH

Table 2: Parameters of the controllers

Parameter	Symbol	Value
Proportional gain of Controller1	K_{p1}	-40
Integral gain of Controller1	K_{i1}	-800000
Proportional gain of Controller2	K_{p2}	-28.5
Integral gain of Controller2	K_{i2}	-233128.8
Proportional gain of Controller3	K_{p3}	-4.5
Integral gain of Controller3	K_{i3}	-6923.1
Proportional gain of Controller4	K_{p4}	-16
Integral gain of Controller4	K_{i4}	-38095.2

For the frequency current control, the output current reference is changed from 12 A to 15 A at 0.015 s and changed from 15 A to 10 A at 0.025 s. Fig. 7 shows the waveforms of the output charging current and the switching frequency. Besides, for the frequency voltage control, the reference of the output charging voltage is changed from 60 V to 55 V at 0.015 s and changed from 55 V to 65 V at 0.025 s. Fig. 8 shows the waveforms of the output charging voltage and the switching frequency. Apparently, by changing the operating frequency to be 87.08 kHz, 85.82 kHz and 87.83 kHz at steady states for the current control and 87.14 kHz, 87.55 kHz and 86.72 kHz at steady states for the voltage control, the output charging current and the output charging voltage are well-regulated to track the references. However, the frequency control may suffer from small oscillations at steady state.

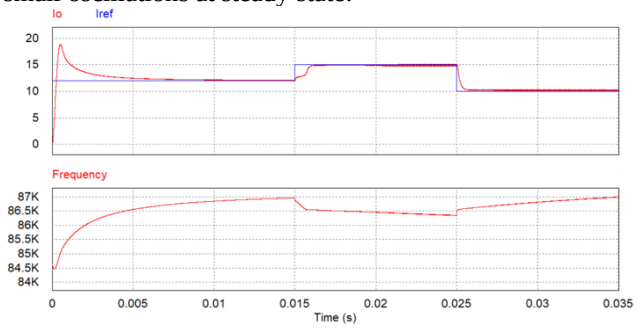

Fig. 7: Output current and switching frequency of the IPT system controlled by the frequency current control.

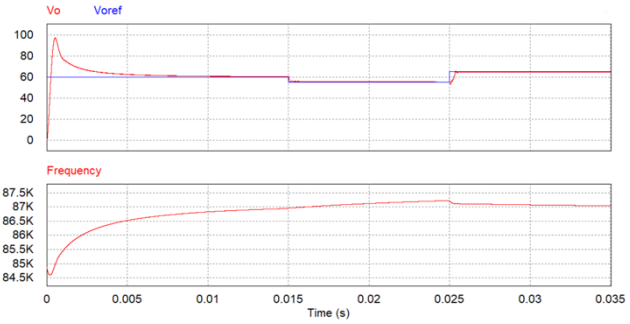

Fig. 8: Output voltage and switching frequency of the IPT system controlled by the frequency voltage control.

For the phase shift current control, the output current reference is also changed from 12 A to 15 A at 0.015 s and changed from 15 A to 10 A at 0.025 s. Fig. 9 shows the waveforms of the output charging current and the corresponding phase shift angle. Besides, for the phase shift voltage control, the reference of output charging voltage is also changed from 60 V to 55 V at 0.015 s and changed from 55 V to 65 V at 0.025 s. The waveforms of the output charging voltage and the corresponding switching frequency are shown in Fig. 10. Obviously, the output charging current and the output charging voltage are well-regulated to track the references by changing the phase shift angle to be -264.7°, -294.9° and -248.8° at steady states for the current control and -265.1°, -256.6° and -273.5° at steady states for the voltage control.

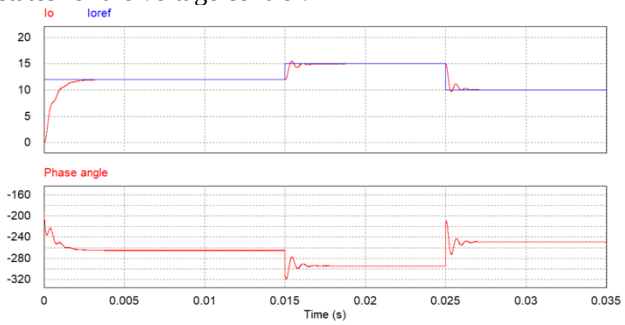

Fig. 9: Output current and shifted angle of the IPT system controlled by the phase shift current control.

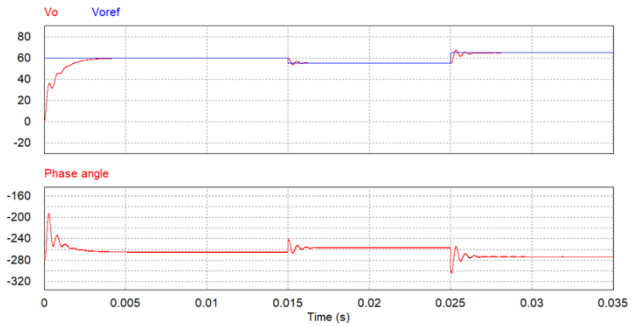

Fig. 10: Output voltage and shifted angle of the IPT system controlled by the phase shift voltage control.

IV. Conclusions

In this paper, both frequency and phase shift control are deigned to charge the Li-ion battery loads of SS-compensated IPT systems in the CC and CV modes. Simulations are carried out in PSIM9.0 to validate that both control strategies can effectively regulate the output charging current and the output charging voltage of a 85 kHz and 200 W IPT system with different charging current and charging voltage references.

REFERENCES

[1] C. C. Mi, G. Buja, S. Y. Choi and C. T. Rim, "Modern advances in wireless power transfer systems for roadway powered electric vehicles," *IEEE Trans. Ind. Electron.*, vol. 63, no. 10, pp. 6533-6545, Oct. 2016.

[2] X. Liu, and S.Y. Hui, "Simulation study and experimental verification of a universal contactless battery charging platform with localized charging features," *IEEE Trans. Power Electron.*, vol. 22, no. 6, pp. 2202-2210, Nov. 2007.

[3] Q. Chen, S. C. Wong, C. K. Tse and X. Ruan, "Analysis, design, and control of a transcutaneous power regulator for artificial hearts," *IEEE Trans. Biomed. Circuits and Syst.*, vol. 3, no. 1, pp. 23-31, Feb. 2009.

[4] Y. Yang, W. X. Zhong, S. Kiratipoonvoot, S. C. Tan, and S. Y. R. Hui, "Dynamic improvement of series-series compensated wireless power transfer systems," *IEEE Trans. Power Electron.*, vol. 33, no. 7, pp. 6351-6360, Jul. 2018.

[5] M. Kim, D. Joo, and B. K. Lee, "Design and control of inductive power transfer system for electric vehicles considering wide variation of output voltage and coupling coefficient," *IEEE Trans. Power Electron.*, vol. 34, no. 2, pp. 1197-1208, Feb. 2019.

[6] Y. Yang, S. C. Tan, and S. Y. R. Hui, "Communication-free control scheme for Qi-compliant wireless power transfer system," in *Energy Conversion Congress and Exposition (ECCE)*, Sept. 2019, pp. 4955-4960.

[7] W. Zhang, S. C. Wong, C. K. Tse and Q. Chen, "Analysis and comparison of secondary series- and parallel-compensated inductive power transfer systems operating for optimal efficiency and load-independent voltage-transfer ratio," *IEEE Trans. Power Electron.*, vol. 29, no. 6, pp. 2979-2990, Jun. 2014.

[8] J. Yin, D. Lin, C. K. Lee, and S. Y. R. Hui, "A systematic approach for load monitoring and power control in wireless power transfer systems without any direct output measurement," *IEEE Trans. Power Electron.*, vol. 30, no. 3, pp. 1657-1667, Mar. 2015.

[9] J. Yin, D. Lin, C. K. Lee, and S. Y. R. Hui, "A systematic approach for load monitoring and power control in wireless power transfer systems without any direct output measurement," *IEEE Trans. Power Electron.*, vol. 30, no. 3, pp. 1657-1667, Mar. 2015.

[10] J. Yin, D. Lin, C. K. Lee, T. Parisini, and S. Y. R. Hui, "Front-end monitoring of multiple loads in wireless power transfer systems without wireless communication systems," *IEEE Trans. Power Electron.*, vol. 31, no. 3, pp. 2510-2517, Mar. 2016.

[11] J. Yin, D. Lin, T. Parisini, and S. Y. R. Hui, "Front-end monitoring of the mutual inductance and load resistance in a series-series compensated wireless power transfer system," *IEEE Trans. Power Electron.*, vol. 31, no. 3, pp. 7339-7352, Oct. 2016.

[12] Y. Yang, Y. Jiang, S. C. Tan, and S. Y. R. Hui, "A freqeuncy-sweep based load monitoring method for weakly-coupled series-series compensated wireless power transfer systems," in *IEEE PELS Workshop on Emerging Technologies: Wireless Power Trasnfer (WoW)*, Jun. 2018, pp. 1-5.

[13] K. Aditya and S. S. Williamson, "Design guidelines to avoid bifurcation in a series–series compensated inductive power transfer system," *IEEE Trans. Ind. Electron.*, vol. 66, no. 5, pp. 3973-3982, May 2019.

[14] Y. Yang, S. C. Tan, and S. Y. R. Hui, "Front-end parameter monitoring method based on two-layer adaptive differential evolution for SS-compensated wireless power transfer systems," *IEEE Trans. Ind. Informat.*, vol. 15, no. 11, pp. 6101-6113, Nov. 2019.

[15] Y. Yang, S. C. Tan, and S. Y. R. Hui, "Fast hardware approach to determining mutual coupling of series-series-compensated wireless power transfer systems with active rectifiers," *IEEE Trans. Power Electron.*, vol. 35, no. 10, pp. 11026-11038, Oct. 2020.